

LETTER • OPEN ACCESS

Symmetry-enforced two-dimensional Dirac node-line semimetals

To cite this article: Peng-Jie Guo *et al* 2023 *Mater. Futures* **2** 011001

View the [article online](#) for updates and enhancements.

You may also like

- [Nonlinear lattice waves in heterogeneous media](#)
T V Lapyeva, M V Ivanchenko and S Flach
- [Relationship between symmetry protected topological phases and boundary conformal field theories via the entanglement spectrum](#)
Gil Young Cho, Ken Shiozaki, Shinsei Ryu et al.
- [Two-dimensional Dirac nodal loop magnons in collinear antiferromagnets](#)
S A Owerre

Letter

Symmetry-enforced two-dimensional Dirac node-line semimetals

Peng-Jie Guo^{1,3} , Chen Peng^{2,3}, Zheng-Xin Liu^{1,*}, Kai Liu^{1,*} and Zhong-Yi Lu^{1,*}¹ Department of Physics and Beijing Key Laboratory of Opto-electronic Functional Materials & Micro-nano Devices, Renmin University of China, Beijing 100872, People's Republic of China² Kavli Institute for Theoretical Sciences, University of Chinese Academy of Sciences, Beijing 100190, People's Republic of ChinaE-mail: liuxp@ruc.edu.cn, kliu@ruc.edu.cn and zlu@ruc.edu.cn

Received 18 November 2022, revised 1 December 2022

Accepted for publication 2 December 2022

Published 28 December 2022



Abstract

Based on symmetry analysis and lattice model calculations, we demonstrate that Dirac nodal line (DNL) can stably exist in two-dimensional (2D) nonmagnetic as well as antiferromagnetic systems. We focus on the situations where the DNLs are enforced by certain symmetries and the degeneracies on the DNLs are inevitable even if spin-orbit coupling is strong. After thorough analysis, we find that five space groups, namely 51, 54, 55, 57 and 127, can enforce the DNLs in 2D nonmagnetic semimetals, and four type-III magnetic space groups (51.293, 54.341, 55.355, 57.380) plus eight type-IV magnetic space groups (51.299, 51.300, 51.302, 54.348, 55.360, 55.361, 57.387 and 127.396) can enforce the DNLs in 2D antiferromagnetic semimetals. By breaking these symmetries, the different 2D topological phases can be obtained. Furthermore, by the first-principles electronic structure calculations, we predict that monolayer YB_4C_4 is a good material platform for studying the exotic properties of 2D symmetry-enforced Dirac node-line semimetals.

Keywords: symmetry-enforced, Dirac nodal line semimetals, nonsymmorphic space group, antiferromagnetic systems

Supplementary material for this article is available [online](#)

1. Introduction

Topological semimetals with symmetry-protected band crossing around the Fermi level have inspired enormous interest in condensed matter physics [1–8]. As a typical family of

topological semimetals, node-line semimetals have high band degeneracy along certain line in the Brillouin zone (BZ) and the resultant drumhead surface states at the boundary. According to the degrees of the band degeneracy, node-line semimetals can be divided into Dirac- and Weyl-type. Usually, the Dirac node-line semimetals are protected by mirror or \mathcal{IT} (\mathcal{I} : space inversion; \mathcal{T} : time reversal) symmetry and are fragile to spin-orbital coupling (SOC). By breaking the different symmetries in the node-line semimetals, the degeneracy can be lifted and a gap may be opened resulting in different topological phases [1, 9–12]. Recently, symmetry enforced DNLs protected by nonsymmorphic symmetry which are robust against strong SOC have been revealed in three-dimensional (3D)

³ These two authors contributed equally to this work.

* Authors to whom any correspondence should be addressed.



Original content from this work may be used under the terms of the [Creative Commons Attribution 4.0 licence](#). Any further distribution of this work must maintain attribution to the author(s) and the title of the work, journal citation and DOI.

Future perspectives

Symmetry-enforced 2D Dirac node-line semimetals are rarely reported. In particular, symmetry-enforced 2D antiferromagnetic Dirac node-line semimetals are firstly proposed in this work. Moreover, a complete list of all the space groups which can protect 2D nonmagnetic and antiferromagnetic Dirac nodal lines against SOC is provided. Future works can focus on predicting symmetry-enforced 2D antiferromagnetic Dirac node-line semimetal materials based on our symmetry analysis and studying their exotic physical properties in experiments.

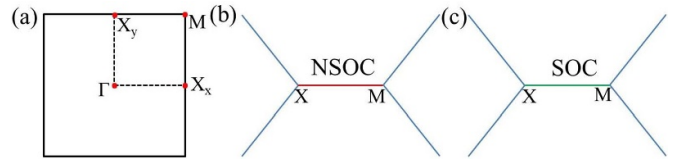


Figure 1. (a) The BZ of square lattice. Nonsymmorphic symmetry protects the Dirac line without (b) and with (c). The red dots represent high-symmetry points. The NSOC represents no spin-orbital coupling.

nonmagnetic and antiferromagnetic systems [13–16]. Then there is an important issue, namely whether or not such Dirac node-lines against strong SOC can exist in 2D nonmagnetic and antiferromagnetic systems.

Such symmetry-enforced DNLs indeed exist in 2D systems. Recent theoretical and experimental studies showed that the tri-layered bismuth taking nonsymmorphic space group symmetry Pmma (51) is a nonmagnetic Dirac node-line semimetal which is robust against strong SOC [17, 18]. Correspondingly, two interesting questions arise. (a) How many space groups can protect Dirac node-lines that are robust against SOC in 2D nonmagnetic systems? (b) Are there stable DNL against SOC in 2D magnetic systems?

To clarify the above questions, we carry out systematic studies based on symmetry analysis and lattice model calculations. We demonstrate that if a nonsymmorphic space group satisfies the four conditions presented in the following, it will enforce 2D DNLs even if SOC is present. Here we adopt the word ‘enforce’ to emphasize having inevitable degeneracy. Actually, the four conditions are the sufficient and necessary conditions for 2D DNLs. Specifically, there are five nonsymmorphic space groups (51, 54, 55, 57, 127) that can enforce DNLs in 2D nonmagnetic semimetals. More importantly, there are twelve magnetic space groups that can enforce DNLs in 2D antiferromagnetic semimetals, including four type-III magnetic space groups (51.293, 54.341, 55.355, 57.380) and eight type-IV magnetic space groups (51.299, 51.300, 51.302, 54.348, 55.360, 55.361, 57.387, 127.396). In the end, using first-principles electronic structure calculations, we predict that monolayer YB₄C₄ and IrPb₃ are symmetry-enforced 2D DNL semimetals.

2. Symmetry analysis

We take the nonsymmorphic space group P4-mbm (127) as an example. The P4-mbm space group includes C_{4z}, C_{2y} (1/2, 1/2, 0), and \mathcal{I} , which yield the point group D_{4h}. Since there is no fractional translation along the z-direction, the space group P4/mbm can support quasi-2D lattice structure, whose BZ is shown in figure 1(a). Clearly, any \mathbf{k} point on the high-symmetry X_y–M axis has the C_{2x}(1/2, 1/2), M_y(1/2, 1/2), and M_z symmetries. Since the \mathcal{T} symmetry always exists in nonmagnetic materials, any \mathbf{k} point in the BZ has the \mathcal{IT} symmetry. Certainly, any \mathbf{k} point on the high-symmetry X_y–M

axis has C_{2x}(1/2, 1/2) \mathcal{IT} symmetry. Without SOC, the square of C_{2x}(1/2, 1/2) \mathcal{IT} is equal to –1 on the high-symmetry X_y–M axis, giving rise to a Kramers degeneracy. The Kramers degenerate band along the X_y–M axis are DNLs, as shown in figure 1(b). With the inclusion of SOC, the relationship between M_y(1/2, 1/2) and M_z changes from commuting to anti-commuting, but the square of C_{2x}(1/2, 1/2) \mathcal{IT} still equals to –1 on the high-symmetry X_y–M axis. Interestingly, the two conditions will guarantee that any band is fourfold degenerate along the high-symmetry X_y–M axis.

To prove it, we assume that the Bloch wave function $\Psi(\mathbf{k})$ is an eigenstate of M_z with eigenvalue i , where \mathbf{k} is any point on the X_y–M axis. Since the square of C_{2x}(1/2, 1/2) \mathcal{IT} equals to –1, $\Psi(\mathbf{k})$ and C_{2x}(1/2, 1/2) $\mathcal{IT}\Psi(\mathbf{k})$ form a pair of Kramers degenerate states. Moreover, the C_{2x}(1/2, 1/2) $\mathcal{IT}\Psi(\mathbf{k})$ is also an eigenstate of M_z with eigenvalue i . On the other hand, due to the anticommutation of M_y(1/2, 1/2) and M_z, the M_y(1/2, 1/2) $\Psi(\mathbf{k})$ and M_y(1/2, 1/2)C_{2x}(1/2, 1/2) $\mathcal{IT}\Psi(\mathbf{k})$ = M_z $\mathcal{IT}\Psi(\mathbf{k})$ are both eigenstates of M_z with eigenvalue $-i$. Since the Bloch Hamiltonian is commutative with C_{2x}(1/2, 1/2), M_y(1/2, 1/2), M_z and \mathcal{IT} , the four states ($\Psi(\mathbf{k})$, M_y(1/2, 1/2) $\Psi(\mathbf{k})$, M_z $\mathcal{IT}\Psi(\mathbf{k})$, C_{2x}(1/2, 1/2) $\mathcal{IT}\Psi(\mathbf{k})$) always form fourfold degeneracy on the X_y–M axis. As a result, a DNL with SOC is formed along the X_y–M axis, as shown in figure 1(c). This conclusion is also verified by the symmetry invariants (–1, –1, –1, –1) of the little group $\mathcal{C}_{2v} \times Z_2^{\mathcal{IT}}$ (here $Z_2^{\mathcal{IT}} = \{E, \mathcal{IT}\}$) on the X_y–M axis. In the (–1, –1, –1, –1) symmetry class, the group $\mathcal{C}_{2v} \times Z_2^{\mathcal{IT}}$ has only one irreducible projective representation whose dimension is 4 (for details see the supplemental material [19]), indicating that the fourfold degeneracy is inevitable and robust against strong SOC, that is symmetry-enforced DNL.

According to the above symmetry analysis, to enforce 2D DNL in case of SOC, a nonsymmorphic space group needs to satisfy four conditions: (a) it has no three different directional fractional translations, which supports two-dimensional lattice structure; (b) the corresponding little co-group is $\mathcal{C}_{2v} \times Z_2^{\mathcal{IT}}$ at the boundary of two-dimensional BZ; (c) there are a fractional translation perpendicular to the C₂ axis and vertical mirror; (d) the horizontal mirror M_z has no fractional translation perpendicular to the C₂ axis or vertical mirror. These four conditions ensure that there is only one four-dimensional irreducible projective representation along the boundary of

BZ. Thus, they are the sufficient and necessary conditions to 2D DNLs. According to the four conditions, there are five nonsymmorphic space groups that can enforce 2D DNLs in case of SOC, which are further proved by the calculated symmetry invariants (see [19] for details). Different from the case of P-mma (51) space group [17, 18], the two boundaries of 2D BZ for the P-bam(55) and P4-mbm (127) space groups host the DNLs.

Another interesting question is whether or not symmetry-enforced 2D DNLs can take place in magnetic systems. The above symmetry analysis on nonmagnetic system demonstrates that a certain nonsymmorphic symmetry $\mathcal{C}_{2v} \times Z_2^{\mathcal{IT}}$ can enforce the DNLs in 2D case. As is known, antiferromagnetic systems may also own the \mathcal{IT} symmetry. If a 2D antiferromagnetic material has the certain nonsymmorphic little group $\mathcal{C}_{2v} \times Z_2^{\mathcal{IT}}$, for example, with symmetry elements $E, M_z, C_{2x}(1/2, 1/2), M_y(1/2, 1/2)$ and \mathcal{IT} , the antiferromagnetic materials must have symmetry-enforced DNL at the boundary of BZ. Likewise, we demonstrate that there are twelve magnetic space groups which can enforce DNLs in 2D antiferromagnetic systems, including four type-III magnetic space groups (51.293, 54.341, 55.355, 57.380) and eight type-IV magnetic space groups (51.299, 51.300, 51.302, 54.348, 55.360, 55.361, 57.387 and 127.396), which can be also protected 2D antiferromagnetic eightfold degenerate fermions without intrinsic SOC [20]. These are further demonstrated by the calculation of the symmetry invariants (see [19] for details). On the other hand, when a DNL crosses the Fermi level, it has advantage to the exotic physical properties in transport experiments. The best is that the symmetry-enforced DNL is formed by the valence and conduction bands. The condition requires that the number of the valence electrons must equal to $4n+2$, here n is a positive integer.

3. Effective lattice model

We now introduce a spinful model with a square lattice including four sublattices for the symmetry-forced 2D DNLs as shown in figure 2(a). The nearest and second nearest hopping terms t and t_2 are labeled with black and blue lines, respectively. To make the lattice nonsymmorphic symmetry, the t_2 term describes the hopping between sublattices 1 and 3 within the unit cell and the hopping between sublattices 2 and 4 in the neighboring unit cell. Then, we add the SOC term indicated by the red arrows describe the nearest hopping in spin-up sector with $\pm i\lambda$ according to the direction, and a minus sign should be added to the SOC amplitude λ in the spin-down sector as shown in figure 2(a). Then we derive the Bloch Hamiltonian

$$\begin{aligned}
 h_{\mathbf{k}} = & 2t \left(\cos \frac{k_y}{2} \tau_1 \sigma_1 + \cos \frac{k_x}{2} \tau_0 \sigma_1 \right) s_0 \\
 & + 2t_2 \cos \frac{k_x + k_y}{2} (\tau_1 \sigma_3 + \tau_1 \sigma_0) s_0 \\
 & + 2t_2 \cos \frac{k_x - k_y}{2} (\tau_1 \sigma_3 - \tau_1 \sigma_0) s_0 \\
 & + 2\lambda \left(\cos \frac{k_x}{2} \tau_0 \sigma_2 - \cos \frac{k_y}{2} \tau_1 \sigma_2 \right) s_3, \quad (1)
 \end{aligned}$$

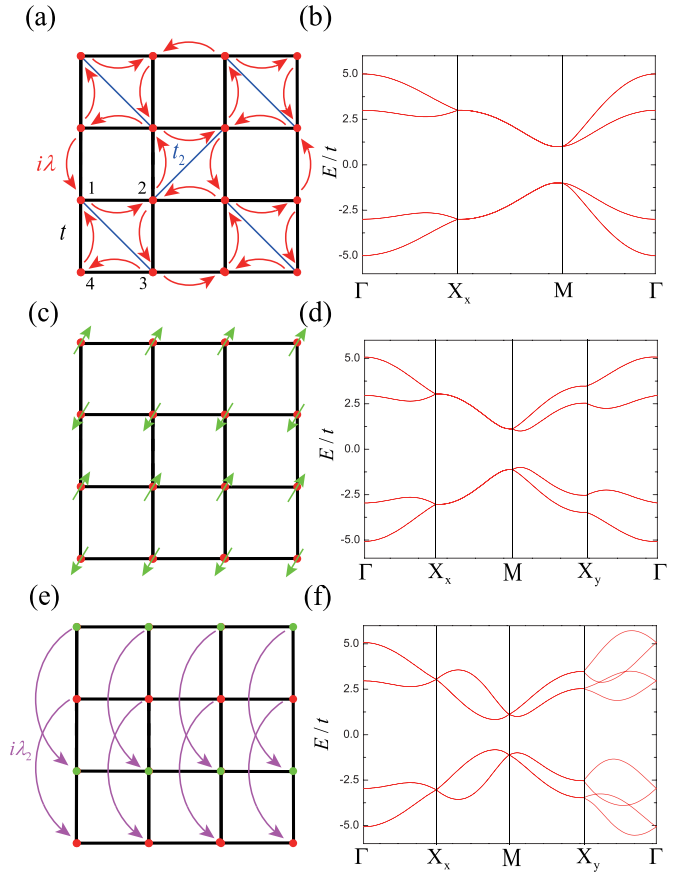


Figure 2. (a) The square lattice with p4/mbm space group symmetry. The black and blue lines indicate the nearest hopping t and second nearest hopping t_2 . The spin-orbital coupling term $i\lambda$, for one spin flavor, is shown by the red arrows. (b) The band structure of lattice model with parameter $\lambda = t_2 = t$ along the high-symmetry directions. Lattice model and band structures: (c)–(d) breaking \mathcal{T} and \mathcal{I} with an out-of plane antiferromagnetic order indicated by the green arrow; (e)–(f) breaking \mathcal{I} symmetry with the chemical potential $\pm\mu$ according to the green/red sites and the spin-orbital coupling term $i\lambda_2$ indicated by the purple arrows.

where both τ and σ are Pauli matrices describing the sub-lattice indices and s are also Pauli matrices describing spin degrees of freedom. The λ term describes SOC, which couples the momentum of the orbital in x/y -direction and the momentum of the spin in z -direction.

The band structure of the lattice model described by equation (1) along the high-symmetry directions is shown in figure 2(b). As revealed by our above symmetry analysis, the symmetry-forced DNLs appear in the X_y - M line as well as the X_x - M line for the C_{4z} . At X_y - M line, $C_{2x}(1/2, 1/2)\mathcal{T} = -e^{-ik_x}\tau_2\sigma_1s_2\mathcal{K}$, $M_y(1/2, 1/2) = ie^{-ik_x/2}\tau_3\sigma_1s_2$ and $M_z = -is_3$ are consistent with the algebraic relationships in the previous discussion and guarantee the fourfold degeneracy at the \mathbf{k} points.

On the other hand, we consider an out-of-plane collinear antiferromagnetic order, which breaks \mathcal{I} and \mathcal{T} but preserves the \mathcal{IT} symmetry as shown in figure 2(c). The out-of-plane collinear antiferromagnetic order can be achieved by adding staggered magnetic field $h_{\mathbf{k}}^m = m\tau_3\sigma_0s_z$ to the above

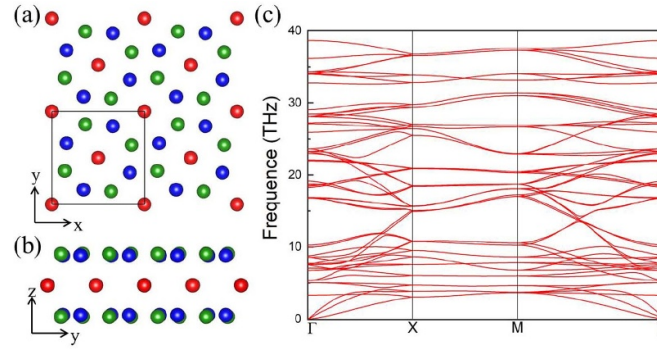


Figure 3. (a) and (b) are the crystal structure of YB_4C_4 viewed along $[001]$ and $[100]$ directions, respectively. The red, blue and green balls represent Y, B and C atoms. (c) Phonon spectrum of monolayer YB_4C_4 along the high-symmetry directions.

lattice model 1, and the antiferromagnetic lattice model has M_z , $C_{2x}(1/2, 1/2)$, $M_y(1/2, 1/2)$, and \mathcal{IT} symmetries. According to our symmetry analysis, these symmetries can enforce the DNLs on the X_x - M axis. Correspondingly, the calculated band structure with $m = 0.5t$ indicates that there does exist symmetry-enforced DNLs on the X_x - M axis as shown in figure 2(d).

Finally, if the \mathcal{I} symmetry is broken but the \mathcal{T} symmetry is preserved, what will be the fate of the symmetry-enforced DNL? Here, we break the inversion symmetry by adding the onsite chemical potential $h_{\mathbf{k}}^{\text{chem}} = \mu\tau_3\sigma_0s_0$ and the spin-orbital coupling along y -direction $h_{\mathbf{k}}^{\lambda_2} = 2\lambda_2 \sin k_y\tau_0\sigma_0s_3$ as shown in figure 2(e). Now, our model has symmetry group $\mathcal{C}_{2v} \otimes Z_2^T$ and the elements of the group are $C_{2x}(1/2, 1/2)$, $M_y(1/2, 1/2)$, M_z , and \mathcal{T} . The corresponding band structure with $\mu = \lambda_2 = 0.5t$ is shown in figure 2(f). The four-fold degeneracy along X_x - M and X_y - M splits due to the broken \mathcal{I} symmetry. However, the Dirac points at the X_x and M points still remain. The four-fold degeneracy can be understood by the similar analysis. At the X_x point, the square of $\mathcal{T} = -i\sigma_3s_2\mathcal{K}$ equals to -1 , giving rise to a Kramers pair formed by ψ and $\mathcal{T}\psi$. And the Kramers pair have the same eigenvalue of $M_z = -is_3$ for the commutation $[M_z, \mathcal{T}] = 0$. Moreover, due to the anticommutation of $M_y(1/2, 1/2) = -\tau_3\sigma_1s_2$ and M_z , ψ and $M_y(1/2, 1/2)\psi$ have the opposite eigenvalues of M_z . In other word, we derive two nonequivalent Kramers pairs:

$$\begin{aligned} & \psi, \mathcal{T}\psi \\ & M_y(1/2, 1/2)\psi, M_y(1/2, 1/2)\mathcal{T}\psi. \end{aligned} \quad (2)$$

The square of $M_y(1/2, 1/2)\mathcal{T} = \tau_0\sigma_2\mathcal{K}$ equals to -1 , meaning that ψ and $M_y(1/2, 1/2)\mathcal{T}\psi$ are also degenerate. So, we finally obtain four bases as shown in equation (2) which constitute a 4D irreducible representation of the little co-group at the X_x point. The Dirac point at the M point can be understood similarly. On the contrary, at the X_y point, the square of $M_y(1/2, 1/2)\mathcal{T} = -\tau_0\sigma_1\mathcal{K}$ equals to 1 , which can not protect the Dirac point. Thus the DNL semimetals can be turned into a Dirac semimetal by breaking the space-inversion symmetry. In fact, the 2D Dirac semimetals against SOC without \mathcal{I} have been studied recently [21].

4. Material calculations

In terms of realistic materials, we focus on the nonsymmorphic P4-mbm (127) space group. The bulk YB_2C_2 has a layered structure with space group P4-mbm and its single crystal was successfully synthesized in experiment [22]. The unit cell of bulk YB_2C_2 contains a BC atomic layer and a Y atomic layer. To preserve the same symmetry as the bulk, the 2D form might be constructed experimentally with two BC atomic layers and one Y atomic layer by the epitaxial growth technique, see figures 3(a) and (b) illustration of the structure. As can be seen, the B and C atoms form octagons with small distortion in the BC atomic layer. In order to confirm the structural stability in 2D form, we calculated the phonon spectrum of monolayer YB_4C_4 . According to figure 3(c), there is no imaginary frequency in the phonon spectrum, indicating the dynamical stability of monolayer YB_4C_4 .

Next, we study the electronic band structure of monolayer YB_4C_4 . Without SOC, monolayer YB_4C_4 is a DNL semimetal protected by the nonsymmorphic $C_{2y}(1/2, 1/2)\mathcal{IT}$ symmetry (figure 4(a)). Since the number of valence electron is 78 ($4 \times 19 + 2$), the Dirac node line crosses the Fermi level. Moreover, there are two Dirac node lines in the vicinity of 0.5 eV above the Fermi level, which are induced by the band inversion and protected by the M_z mirror symmetry (figure 4(a)). When the SOC effect is included, just like the above symmetry analysis, the DNL along the X - M direction is still robust (figure 4(b)). To show the DNL more clearly, we calculated the 2D electronic band structure. From figure 4(c), the Dirac node line has linear dispersion along the k_x direction but shows quadratic dispersion along the line direction, which is consistent with our previous theoretical analysis [18]. Due to the C_4 symmetry, another boundary in the 2D BZ must also host symmetry-enforced DNLs.

On the other hand, since these bands around the Fermi level mainly come from the contribution of the p orbitals of B and C atoms, the energy scale of SOC is less than 1 meV which is too small to show the robustness of the DNL against SOC. To better show the robustness, we find another material IrPb_3 with strong SOC in the database of two-dimensional materials [23]. The calculated results indicate that IrPb_3 is a symmetry-enforced 2D Dirac node-line semimetal [19]. Interestingly,

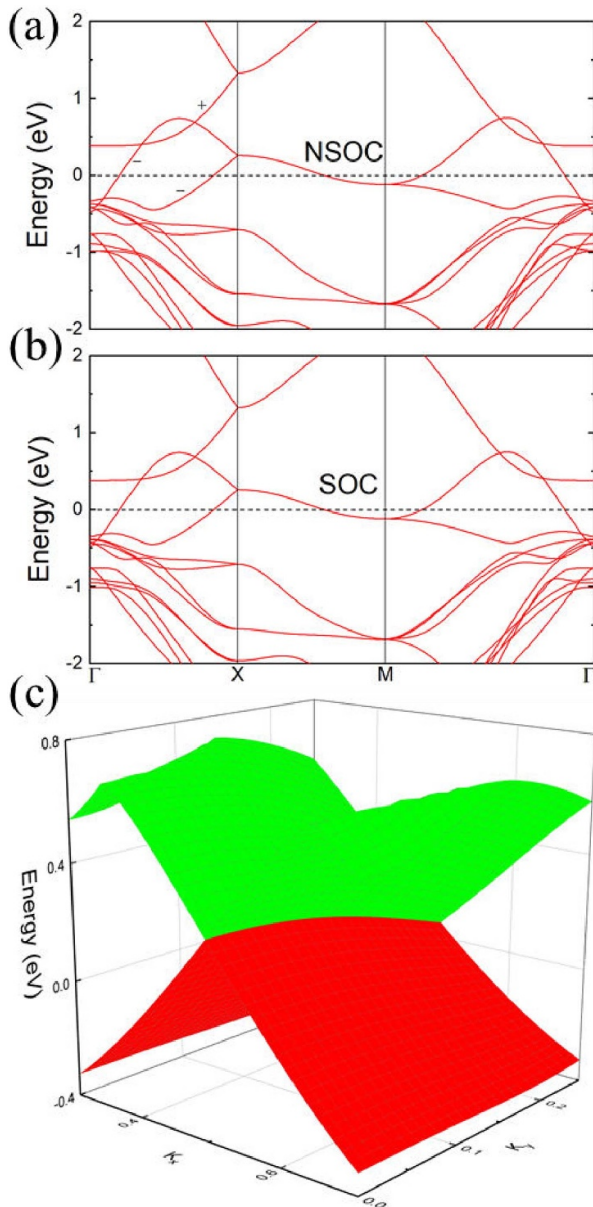


Figure 4. The electronic band structures of monolayer YB_4C_4 along the high-symmetry direction (a) without and (b) with SOC. The both '+' and '-' represent eigenvalue of M_z . (c) The three-dimensional electronic band structure. The NSOC represents no spin-orbital coupling.

the 2D single Dirac without the \mathcal{I} symmetry is obtained by breaking the \mathcal{I} symmetry for IrPb_3 [19]. Moreover, the single Dirac semimetal without \mathcal{I} symmetry is firstly proposed and implemented. On the other hand, the single Dirac semimetals are at the phase boundary of topological insulator and trivial insulator [24].

5. Summary

Based on symmetry analysis, lattice model calculations, and first-principles electronic structure calculations, we obtain

four main results: (a) symmetry-enforced 2D Dirac node-line semimetals can exist not only in nonmagnetic systems but also in antiferromagnetic systems; (b) there are seventeen Shubonikov space groups enforcing the DNL in 2D systems against SOC, including five grey (namely type-II magnetic) space groups (51, 54, 55, 57, 127), four type-III magnetic space groups (51.293, 54.341, 55.355, 57.380) and eight type-IV magnetic space groups (51.299, 51.300, 51.302, 54.348, 55.360, 55.361, 57.387 and 127.396); (c) the symmetry-enforced 2D Dirac node-line semimetals can be turned into a different topological phase by breaking certain symmetry; (d) we predict that monolayer YB_4C_4 and IrPb_3 are 2D symmetry-enforced Dirac node-line semimetals and the former may be a good platform for further study of the exotic transport properties of symmetry-enforced 2D Dirac node-line semimetals.

Acknowledgments

P-J Guo was financially supported by the National Natural Science Foundation of China (No.12204533). K Liu was supported by the National Key R&D Program of China (Grant No. 2017YFA0302903), the Fundamental Research Funds for the Central Universities (CN), and the Research Funds of Renmin University of China (Grant No. 19XNLG13). Z X Liu was supported by the National Natural Science Foundation of China (Grant Nos. 12134020 and 11974421). Z Y Lu was supported by the National Natural Science Foundation of China (Grant No. 11934020).

ORCID iD

Peng-Jie Guo  <https://orcid.org/0000-0003-2705-612X>

References

- [1] Weng H, Dai X and Fang Z 2016 Topological semimetals predicted from first-principles calculations *J. Phys.: Condens. Matter* **28** 303001
- [2] Soluyanov A A, Gresch D, Wang Z, Wu Q, Troyer M, Dai X and Bernevig B A 2015 Type-II Weyl semimetals *Nature* **527** 495
- [3] Huang H, Zhou S and Duan W 2016 Type-II Dirac fermions in the PtSe_2 class of transition metal dichalcogenides *Phys. Rev. B* **94** 121117
- [4] Guo P-J, Yang H-C, Liu K and Lu Z-Y 2017 Type-II Dirac semimetals in the YPd_2Sn class *Phys. Rev. B* **95** 155112
- [5] Wieder B J, Kim Y, Rappe A M and Kane C L 2016 Double Dirac semimetals in three dimensions *Phys. Rev. Lett.* **116** 186402
- [6] Bradlyn B, Cano J, Wang Z, Vergniory M G, Felser C, Cava R J and Bernevig B A 2016 Beyond Dirac and Weyl fermions: unconventional quasiparticles in conventional crystals *Science* **353** aaf5037
- [7] Weng H, Fang C, Fang Z and Dai X 2016 Topological semimetals with triply degenerate nodal points in θ -phase tantalum nitride *Phys. Rev. B* **93** 241202

- [8] Guo P-J, Yang H-C, Liu K and Lu Z-Y 2018 Triply degenerate nodal points in RRh_6Ge_4 ($R = Y, La, Lu$) *Phys. Rev. B* **98** 045134
- [9] Fang C, Chen Y, Kee H-Y and Fu L 2015 Topological nodal line semimetals with and without spin-orbital coupling *Phys. Rev. B* **92** 081201
- [10] Weng H, Liang Y, Xu Q, Yu R, Fang Z, Dai X and Kawazoe Y 2015 Topological node-line semimetal in three-dimensional graphene networks *Phys. Rev. B* **92** 045108
- [11] Zhang X, Yu Z-M, Sheng X-L, Yang H Y and Yang S A 2017 Coexistence of four-band nodal rings and triply degenerate nodal points in centrosymmetric metal diborides *Phys. Rev. B* **95** 235116
- [12] Yu R, Weng H, Fang Z, Dai X and Hu X 2015 Topological node-line semimetal and Dirac semimetal state in antiperovskite Cu_3PdN *Phys. Rev. Lett.* **115** 036807
- [13] Li S, Liu Y, Wang S-S, Yu Z-M, Guan S, Sheng X-L, Yao Y and Yang S A 2018 Nonsymmorphic-symmetry-protected hourglass Dirac loop, nodal line and Dirac point in bulk and monolayer X_3SiTe_6 ($X = Ta, Nb$) *Phys. Rev. B* **97** 045131
- [14] Gao Y, Guo P-J, Liu K and Lu Z-Y 2020 $RRuB_2$ ($R = Y, Lu$), topological superconductor candidates with hourglass-type Dirac ring *Phys. Rev. B* **102** 115137
- [15] Shao D and Fang C 2020 Filling-enforced Dirac nodal loops in nonmagnetic systems and their evolutions under various perturbations *Phys. Rev. B* **102** 165135
- [16] Yang J, Fang C and Liu Z-X 2021 Symmetry-protected nodal points and nodal lines in magnetic materials *Phys. Rev. B* **103** 245141
- [17] Cui X, Li Y, Guo D, Guo P, Lou C, Mei G, Lin C, Tan S, Zhengxin L, Liu K, Lu Z, Petek H, Cao L, Ji W and Feng M 2020 Two-dimensional Dirac nodal-line semimetal against strong spin-orbit coupling in real materials **2012** 15220 (arXiv:2012.15220)
- [18] Guo D, Guo P, Tan S, Feng M, Cao L, Liu Z-X, Liu K, Lu Z and Ji W 2022 Two-dimensional Dirac-line semimetals resistant to strong spin-orbit coupling *Sci. Bull.* **67** 1954
- [19] For details see the supplemental material
- [20] Guo P-J, Wei Y-W, Liu K, Liu Z-X and Lu Z-Y 2021 Eightfold degenerate fermions in two dimensions *Phys. Rev. Lett.* **127** 176401
- [21] Jin Y J, Zheng B B, Xiao X L, Chen Z J, Xu Y and Xu H 2020 Two-dimensional Dirac semimetals without inversion symmetry *Phys. Rev. Lett.* **125** 116402
- [22] Reckeweg O and DiSalvo F J 2014 Different structural models of YB_2C_2 and GdB_2C_2 on the basis of single-crystal x-ray data *Z. Nat.forsch. B* **69** 289
- [23] Zhou J *et al* 2019 2dmatpedia, an open computational database of two-dimensional materials from top-down and bottom-up approaches *Sci. Data* **6** 86
- [24] Young S M and Kane C L 2015 Dirac semimetals in two dimensions *Phys. Rev. Lett.* **115** 126803